eLIFE elifesciences.org

RESEARCH ARTICLE

Figures and figure supplements

Specific structural elements of the T-box riboswitch drive the two-step binding of the tRNA ligand

Jiacheng Zhang *et al*

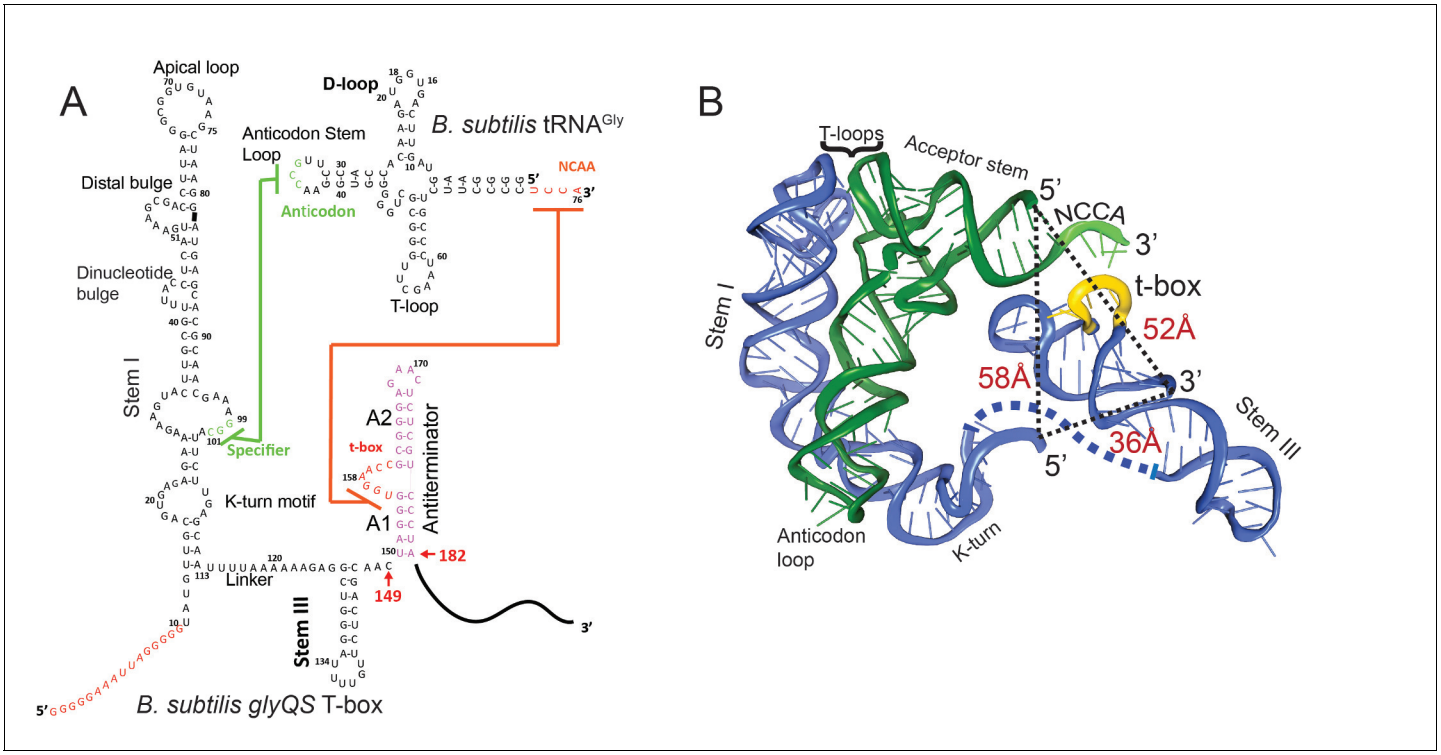

Figure 1. Secondary and tertiary structures of *B. subtilis glyQS* T-box riboswitch and tRNA^{Gly}. (**A**) Secondary structure diagrams of the *B. subtilis glyQS* T-box riboswitch and *B. subtilis* tRNA^{Gly} used in this study. Green and orange lines indicate interactions between the T-box specifier loop and the tRNA anticodon and between the T-box t-box sequence and the tRNA 3′ NCCA, respectively. For the *glyQS* T-box sequence, the nucleotides in red were added for surface immobilization. (**B**) Ribbon diagram of a model of a complex between the *B. subtilis glyQS* T-box riboswitch (blue) and *B. subtilis* tRNA^{Gly} (green) based on SAXS data (***Chetnani and Mondragón, 2017***). Distances between the 5′ and 3′ ends of the T-box and the 5′ end of the tRNA^{Gly} are shown (black dash lines). The NCCA sequence at the 3′ end of the tRNA is shown in light green and the t-box sequence in the T-box is shown in yellow.

DOI: https://doi.org/10.7554/eLife.39518.003

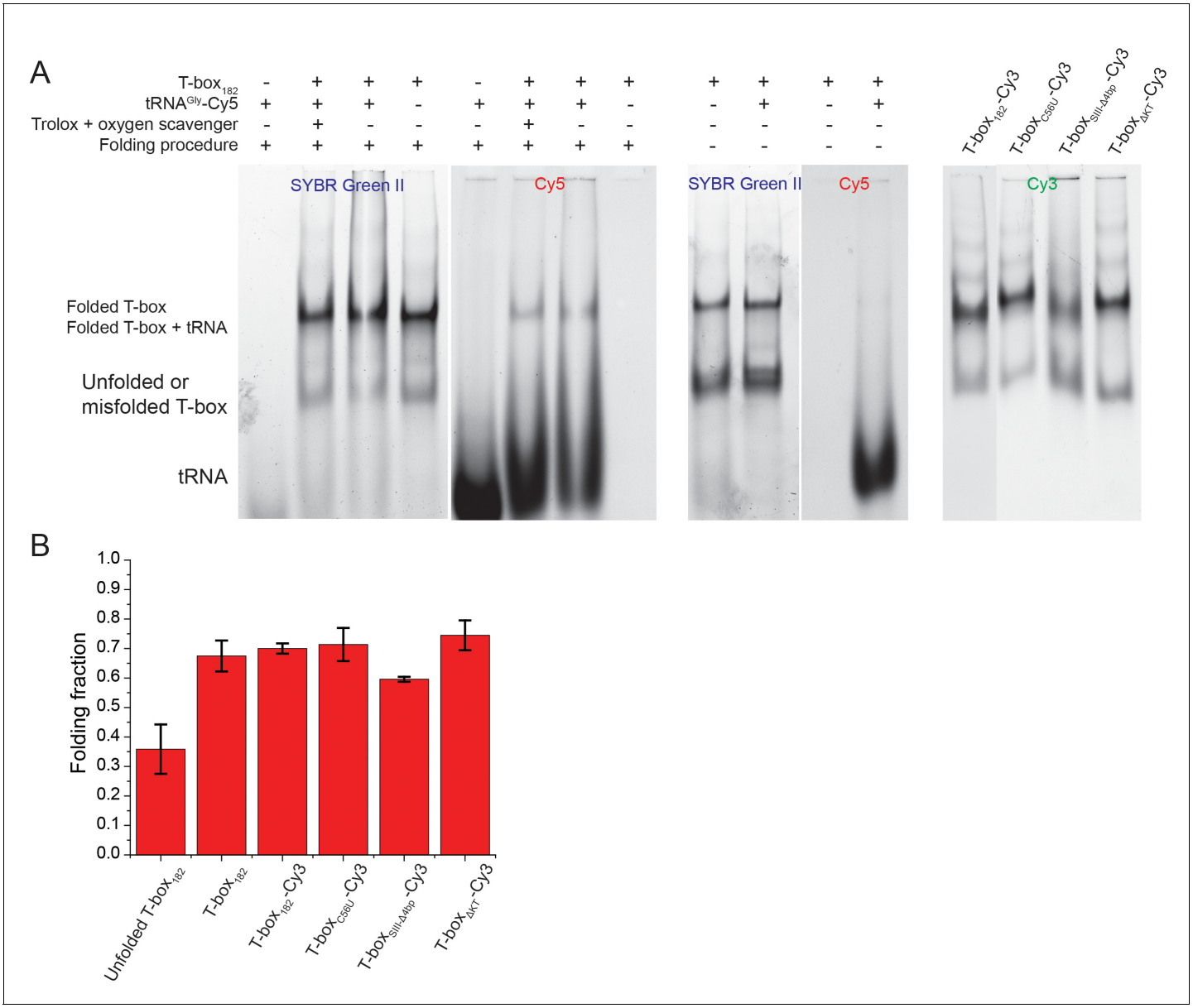

Figure 1—figure supplement 1. Native gel electrophoresis analysis of the folding of T-box constructs and binding of tRNA. (**A**) T-box constructs and tRNA were refolded as described in the Materials and methods. Folding of tRNA is close to 100%, whereas a fraction of T-box is not folded in each construct. However, tRNA-Cy5 only binds to the correctly folded fraction; therefore, the residual unfolded or misfolded fraction does not interfere with our smFRET data collection or analysis. In addition, adding an oxygen scavenger and triplet-state quencher does not interfere with the binding of tRNA-Cy5. All T-box mutants show comparable folding efficiency as the wild-type $T\text{-}box_{182}$. (**B**) Quantification of the folding efficiency was performed by ImageJ (***Schneider et al., 2012***) with background subtraction. Error bars represent standard deviation from at least three independent experiments.
DOI: https://doi.org/10.7554/eLife.39518.004

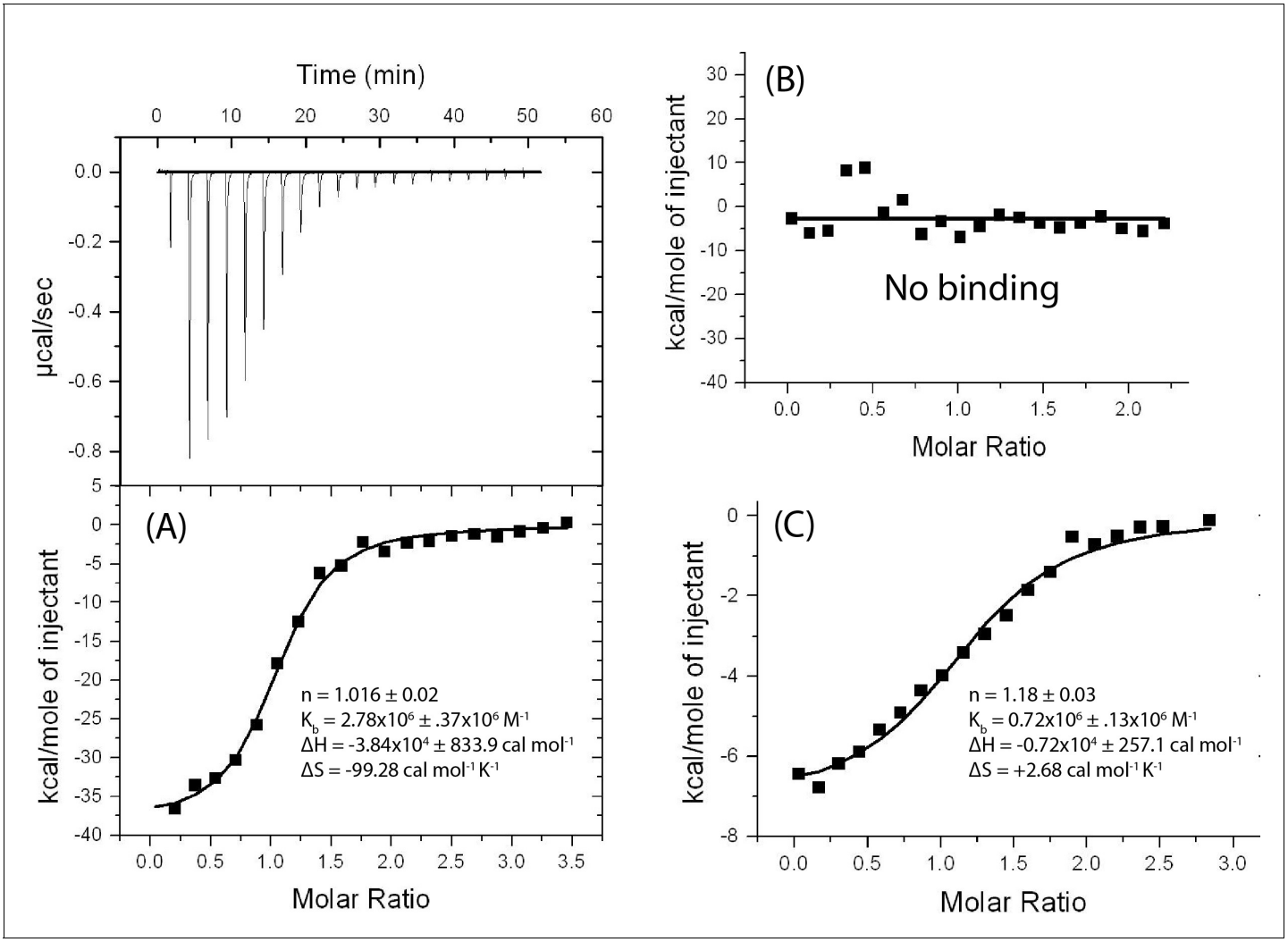

Figure 1—figure supplement 2. Isothermal Titration Calorimetry (ITC) of tRNA binding to T-box$_{182}$. T-box$_{182}$ contains extensions at both 5′ and 3′ ends with (**A**) unlabeled tRNA^{Gly} in 10 mM $MgCl_2$ buffer, (**B**) unlabeled tRNA^{Gly} in 1 mM $MgCl_2$ buffer and (**C**) 5′-Cy5 labelled tRNA^{Gly} in 10 mM $MgCl_2$ buffer. (**A**) is a representative ITC profile in which the upper panel shows the heat change due to successive injections of tRNA^{Gly} to a T-box$_{182}$ construct with extensions at both the 5′ and 3′ ends (***Supplementary file 1***) and the lower panel shows the binding isotherm obtained by integrating the heat change associated with each injection and plotting it as a function of molar ratio of tRNA^{Gly} to T-box$_{182}$. (**B**) and (**C**) depict only the integrated binding isotherm. The first injection of the titration in all three ITC experiments was performed by injecting 0.5 µL of tRNA^{Gly} to minimize contribution of any artifact associate with loading the syringe. A curve was fitted to the integrated data using a single-site model with Origin 5.0 (OriginLab). Thermodynamic parameters are derived from a best fit curve ±minimized fitting error by non-linear regression analysis. (**A**) shows that unlabeled tRNA^{Gly} in 10 mM $MgCl_2$ buffer binds with an affinity ($1/K_b$) of 360 nM which is comparable to the one reported for a similar construct (209 nM) (***Zhang and Ferré-D'Amaré, 2013***), but without the extensions. The experiment therefore shows that the extensions have a negligible effect on tRNA binding. (**B**) shows that in 1mM$MgCl_2$ buffer, tRNA^{Gly} does not bind to the T-box, suggesting that the T-box-tRNA interaction is strongly dependent on Mg^{2+} concentration. (**C**) shows that the addition of Cy5 fluorophore to the 5′ end of tRNA^{Gly} is only slightly detrimental for optimal binding to the T-box with ~4 fold reduction in affinity.

DOI: https://doi.org/10.7554/eLife.39518.005

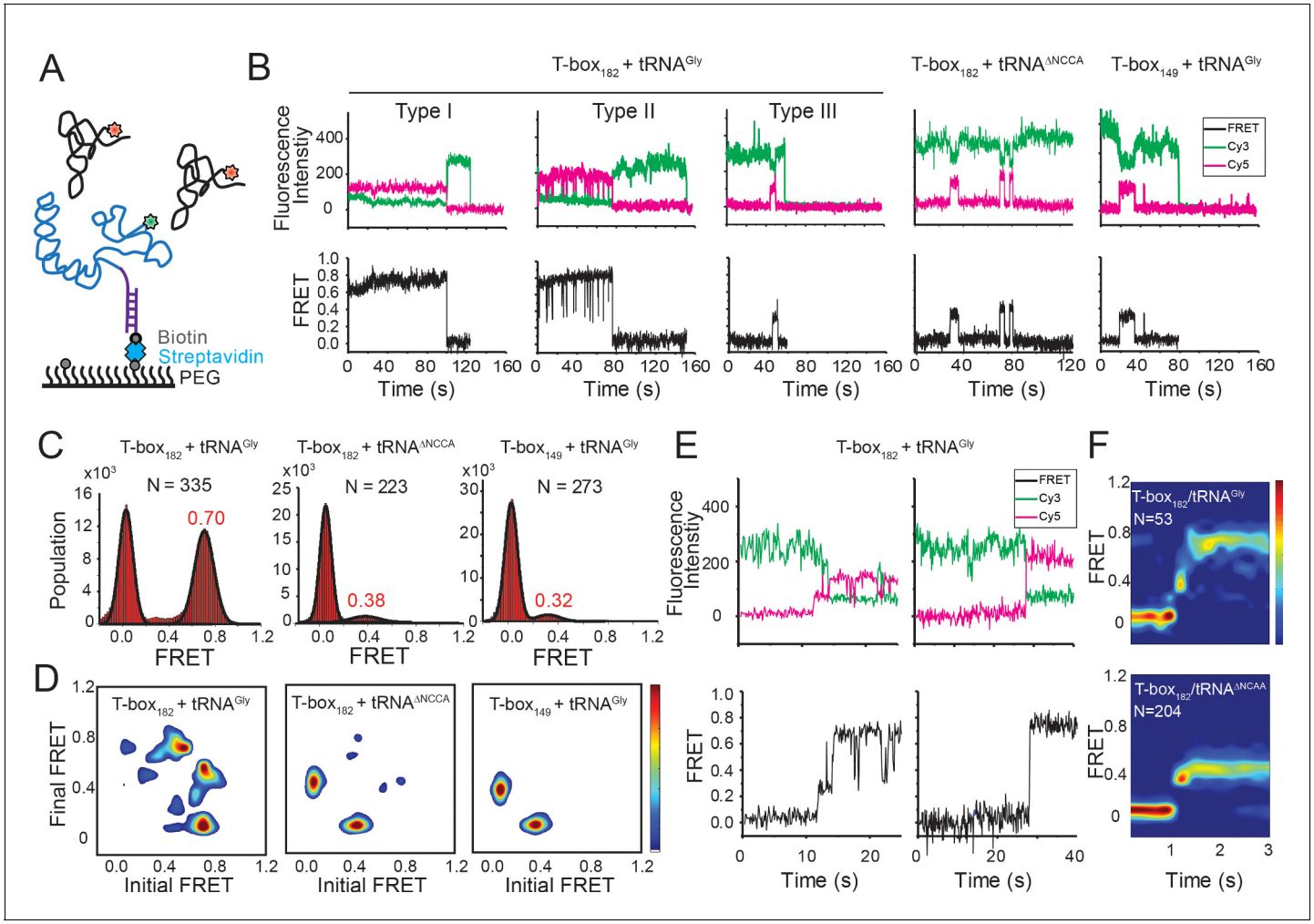

Figure 2. Two-step binding of uncharged tRNA to the *glyQS* T-box riboswitch. (**A**) FRET labeling scheme for the T-box and tRNA. Cy3 (green star) and Cy5 (red star) fluorophores are attached at the 3′ of the T-box (blue) and the 5′ of the tRNA (black), respectively. *glyQS* T-box riboswitch molecules are anchored on slides through a biotinylated DNA probe (purple) hybridized to a 5′ extension sequence on the T-box. (**B**) smFRET *vs.* time trajectories of T-box$_{182}$-Cy3(3′) with tRNA^{Gly}-Cy5, T-box$_{182}$-Cy3(3′) with tRNA$^{\Delta NCCA}$-Cy5 and T-box$_{149}$-Cy3(3′) with tRNA^{Gly}-Cy5. Cy3 and Cy5 fluorescence intensity traces (upper panel), and their corresponding smFRET traces calculated as I_{Cy5} / ($I_{Cy3+}I_{Cy5}$) (lower panel). (**C**) One-dimensional FRET histograms. FRET peaks are fit with a Gaussian distribution (black curve) and the peak centers are shown in red. 'N' denotes the total number of traces in each histogram from three independent experiments. (**D**) Transition density plot (TDP). Contours are plotted from white (less than 15% of the maximum population) to red (more than 85% of the maximum population). TDPs are generated from all smFRET traces from three independent experiments. (**E**) Representative smFRET trajectories showing real-time binding of tRNA^{Gly}-Cy5 to T-box$_{182}$-Cy3(3′) in a steady-state measurement. Traces showing transitions from the unbound state (0 FRET) to fully bound state (0.7 FRET) through the partially bound state (0.4 FRET) (left) and unbound state directly to fully bound state (right). (**F**) Surface contour plot of time-evolved FRET histogram of T-box$_{182}$-Cy3(3′) with tRNA^{Gly}-Cy5 (top) and tRNA$^{\Delta NCCA}$-Cy5 (bottom). Contours are plotted from blue (less than 5% of the maximum population) to red (more than 75% of the maximum population). 'N' denotes the total number of traces in each histogram from three independent experiments, which are a subset of traces showing real-time binding events in the steady-state measurements. Total numbers of traces in steady-state measurements are indicated in (C). Traces that reach the 0.7 FRET state (cutoff >0.55) are included in the plot for tRNA^{Gly}-Cy5 to reveal better the transition from the 0.4 to the 0.7 FRET state. Time-evolved FRET histograms of all traces are shown in ***Figure 2—figure supplement 4D*** for comparison.

DOI: https://doi.org/10.7554/eLife.39518.006

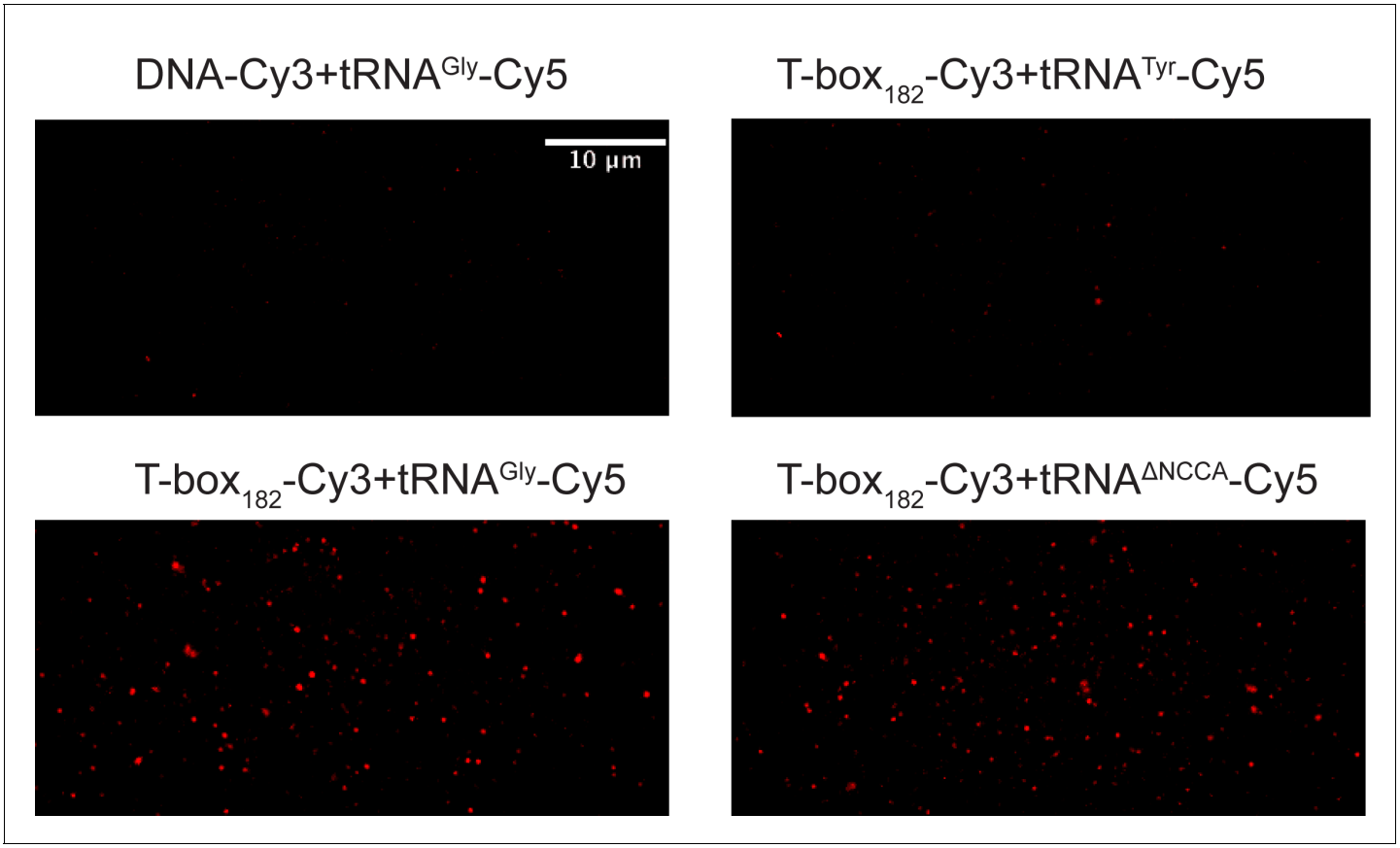

Figure 2—figure supplement 1. Representative images of smFRET data for T-box-Cy3(3') and tRNA-Cy5 binding. Images were created by maximum intensity projection of Cy5 emission of the time-lapse images and therefore report on the binding events of tRNA-Cy5 to the surface tethered T-box. A DNA oligo labeled with Cy3 is used as a negative control for non-specific binding or signal. Loading tRNA^{Tyr}-Cy5 to pre-immobilized T-box-Cy3(3') only generates background level of Cy5 signals in the maximum intensity projection similar to the negative control, and these nonspecific Cy5 signals do not generate any smFRET traces.

DOI: https://doi.org/10.7554/eLife.39518.007

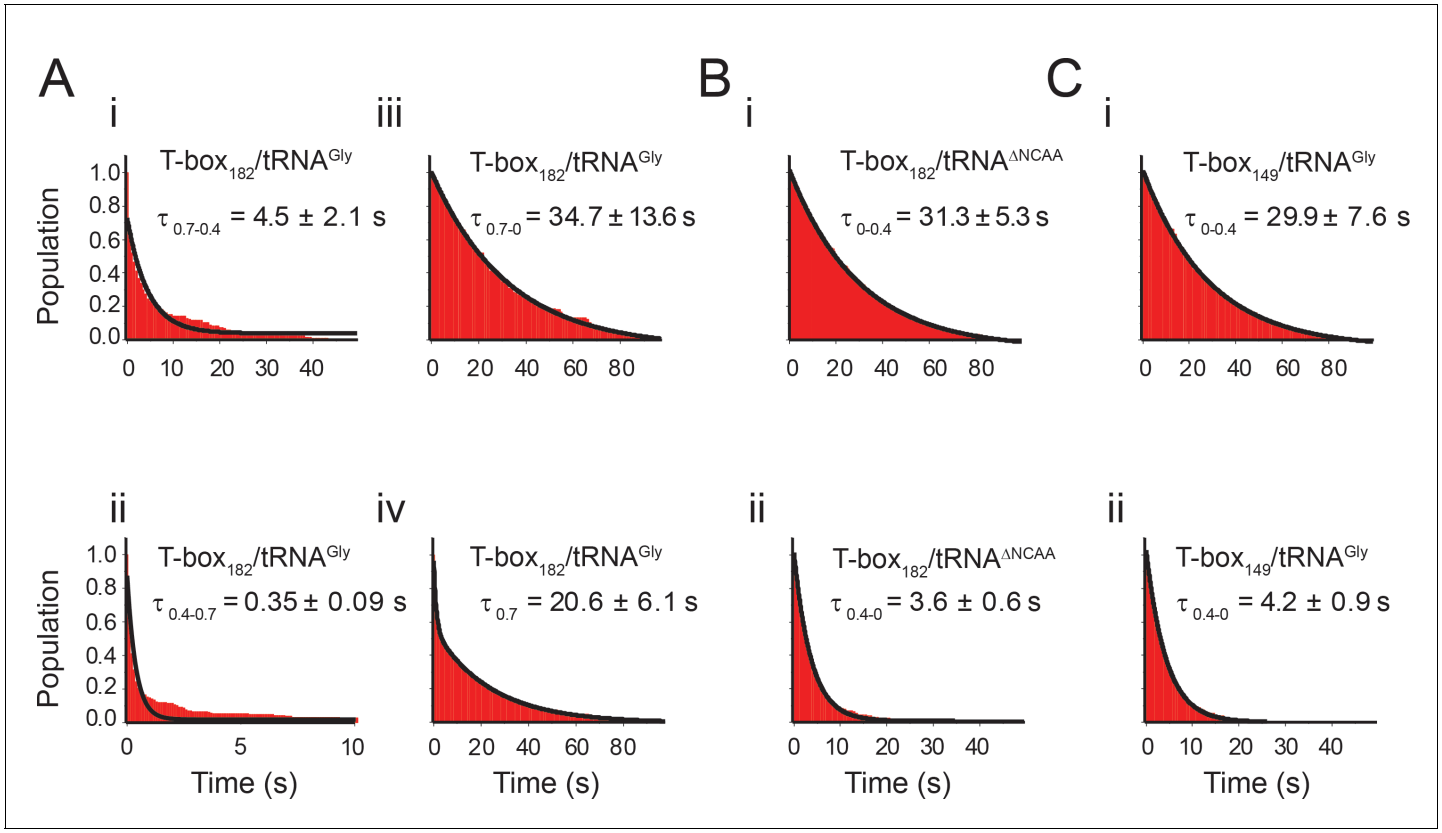

Figure 2—figure supplement 2. Lifetime analyses of *glyQS* T-box-Cy3(3') and tRNA-Cy5 interaction. (**A**) Dwell time of i) 0.7 FRET state to 0.4 FRET state, ii) 0.4 FRET state to 0.7 FRET state, iii) 0.7 FRET state to 0 FRET state, and iv) 0.7 FRET state to other FRET states of T-box$_{182}$-Cy3(3') with tRNA^{Gly}-Cy5. Histograms of i), ii), and iii) are fit with a single-exponential decay function (black curve) and iv) is fit with a double exponential decay function to generate the population-weighted average lifetime of the 0.7 FRET state ($\tau_{0.7}$), as molecules can transit from 0.7 FRET state to both 0.4 FRET state occasionally, and 0 FRET state upon fluorophore photobleaching. (**B**) Dwell time of i) 0 FRET to 0.4 FRET state and ii) 0.4 FRET state to 0 FRET of T-box$_{182}$-Cy3(3') with tRNA$^{\Delta NCCA}$-Cy5. Histograms are fit with a single-exponential decay function (black curve). (**C**) Dwell time of i) 0 FRET state to 0.4 FRET state and ii) 0.4 FRET state to 0 FRET state of T-box$_{149}$-Cy3(3') with tRNA^{Gly}-Cy5. Histograms are fit with a single-exponential decay function (black curve). Mean ±standard deviation (S.D.) are calculated from three independent measurements.

DOI: https://doi.org/10.7554/eLife.39518.008

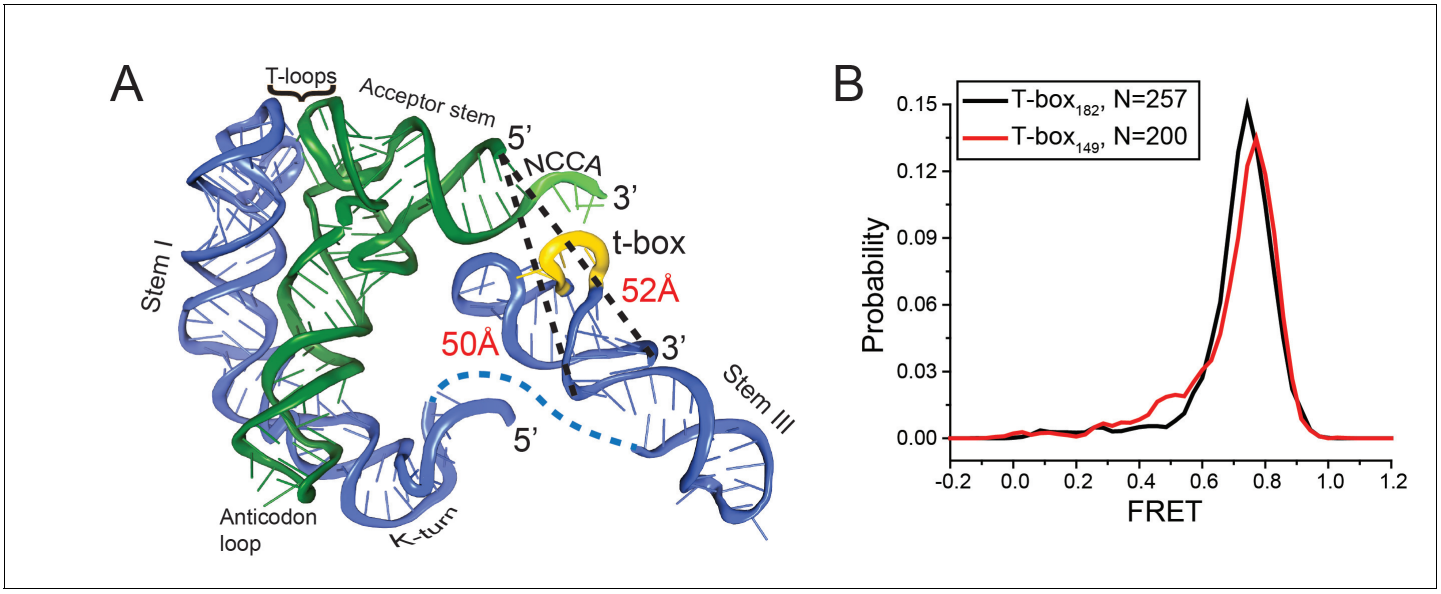

Figure 2—figure supplement 3. Intra-T-box FRET of T-box$_{182}$ and T-box$_{149}$. (**A**) Ribbon diagram of a complex of the *B. subtilis glyQS* T-box riboswitch and uncharged tRNA^{Gly} (***Chetnani and Mondragón, 2017***). Distances from the 5′ end of the tRNA to the 3′ end of the anti-terminator (T-box$_{182}$) and to the 3′ end of Stem III (T-box$_{149}$) are marked. (**B**) One dimensional FRET histograms of intra-T-box pair of T-box$_{182}$ (black) and T-box$_{149}$ (red) with Cy3 attached directly to the 3′ end of the T-box and Cy5 attached to the oligo hybridized to the 5′ extension of the T-box. Only the first 50 data points of the FRET trajectories are used to plot the histogram to eliminate the zero FRET resulting from Cy5 photobleaching. 'N' denotes the total number of traces in each histogram from two independent experiments.

DOI: https://doi.org/10.7554/eLife.39518.009

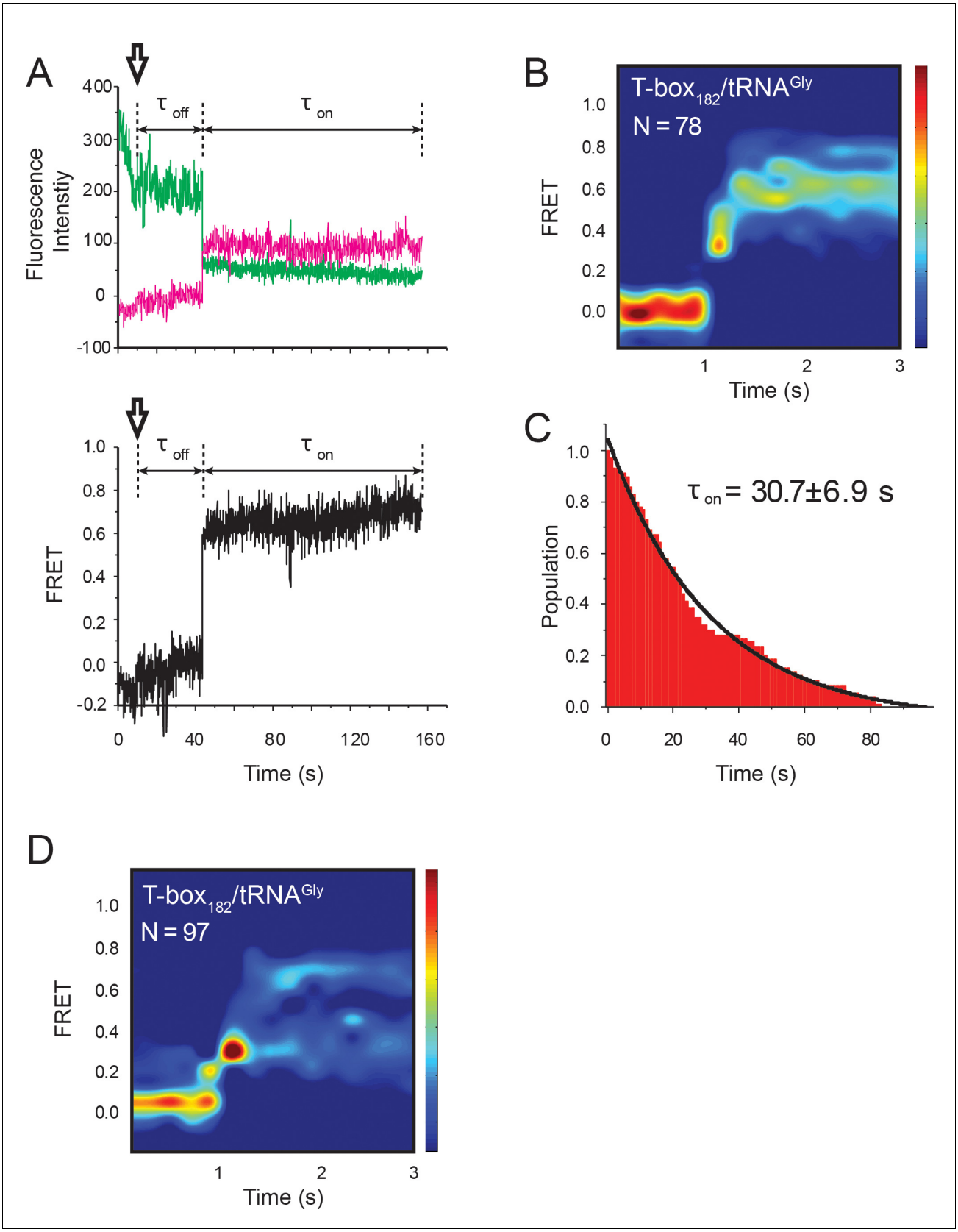

Figure 2—figure supplement 4. Real-time flow experiment of the T-box$_{182}$-Cy3(3′) and tRNA^{Gly}-Cy5. (**A**) smFRET trajectories of T-box$_{182}$-Cy3(3′) and tRNA^{Gly}-Cy5. Black arrows represent the time point when tRNA^{Gly}-Cy5 is flowed through the imaging area. Dwell time of unbound state (T_{off}) was

Figure 2—figure supplement 4 continued on next page

Figure 2—figure supplement 4 continued

calculated as the time between starting point and first FRET transition. (**B**) Surface contour plot of time-evolved FRET histogram of the flow experiment. 'N' denotes the total number of traces in each histogram from two independent experiments. (**C**) Histogram of τ_{off} and its single-exponential decay fitting. Mean ±S.D. are calculated from two independent measurements. (**D**) Surface contour plot of time-evolved FRET histogram of all traces showing real-time binding events, including the traces that are unable to reach the 0.7 FRET state. The same data sets are used in ***Figure 2F***. 'N' denotes the total number of traces in each histogram from three independent experiments, which are a subset of traces showing real-time binding event in the steady-state measurements. Total numbers of traces in the steady-state measurements are indicated in ***Figure 2B***. Contours in (**B**) and (**D**) are plotted in the same way as in ***Figure 2F***.

DOI: https://doi.org/10.7554/eLife.39518.012

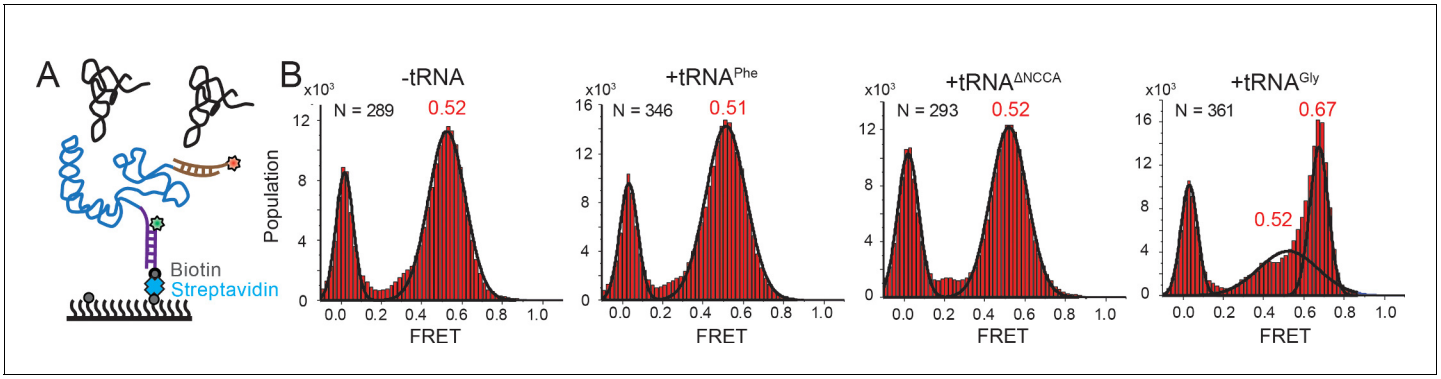

Figure 3. Conformational changes following tRNA binding in the *glyQS* T-box riboswitch revealed by an intra-T-box FRET pair. (**A**) Intra-T-box FRET scheme. Cy3 (green star) and Cy5 (red star) are attached at the 5′ and 3′ extensions of T-box (blue), respectively. (**B**) One-dimensional FRET histograms of T-box$_{182}$ alone, with tRNA^{Phe}, with tRNA$^{\Delta NCCA}$, and with tRNA^{Gly}. 'N' denotes the total number of traces in each histogram from three independent experiments.

DOI: https://doi.org/10.7554/eLife.39518.017

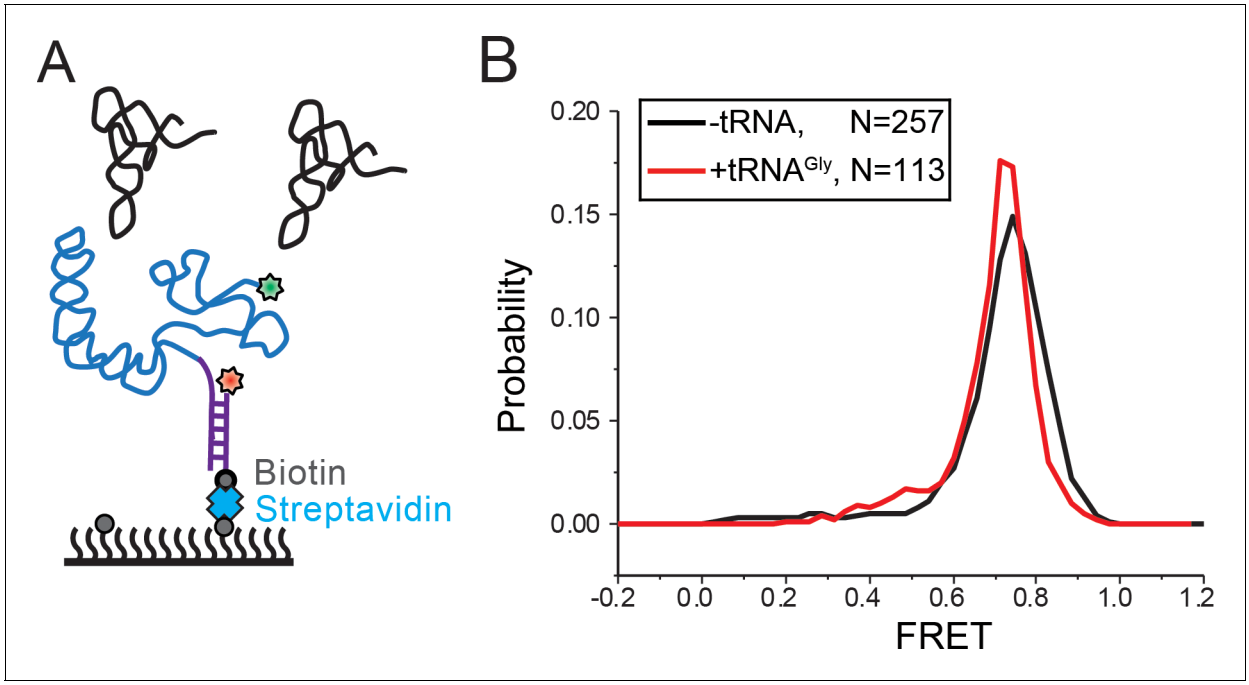

Figure 3—figure supplement 1. Intra-T-box FRET of T-box$_{182}$ in response to tRNA binding. (**A**) Cy5 (red star) and Cy3 (green star) are attached at the 5′ extension of the T-box (blue) and the 3′ end of the T-box, respectively. (**B**) One dimensional FRET histograms of intra-T-box pair of T-box$_{182}$ alone (black) and with tRNA^{Gly} (red). 'N' denotes the total number of traces in each histogram from all independent experiments. For '-tRNA' case, two independent measurements were performed. For '+tRNA^{Gly}' case, as no difference was detected, we only performed the measurement once.
DOI: https://doi.org/10.7554/eLife.39518.018

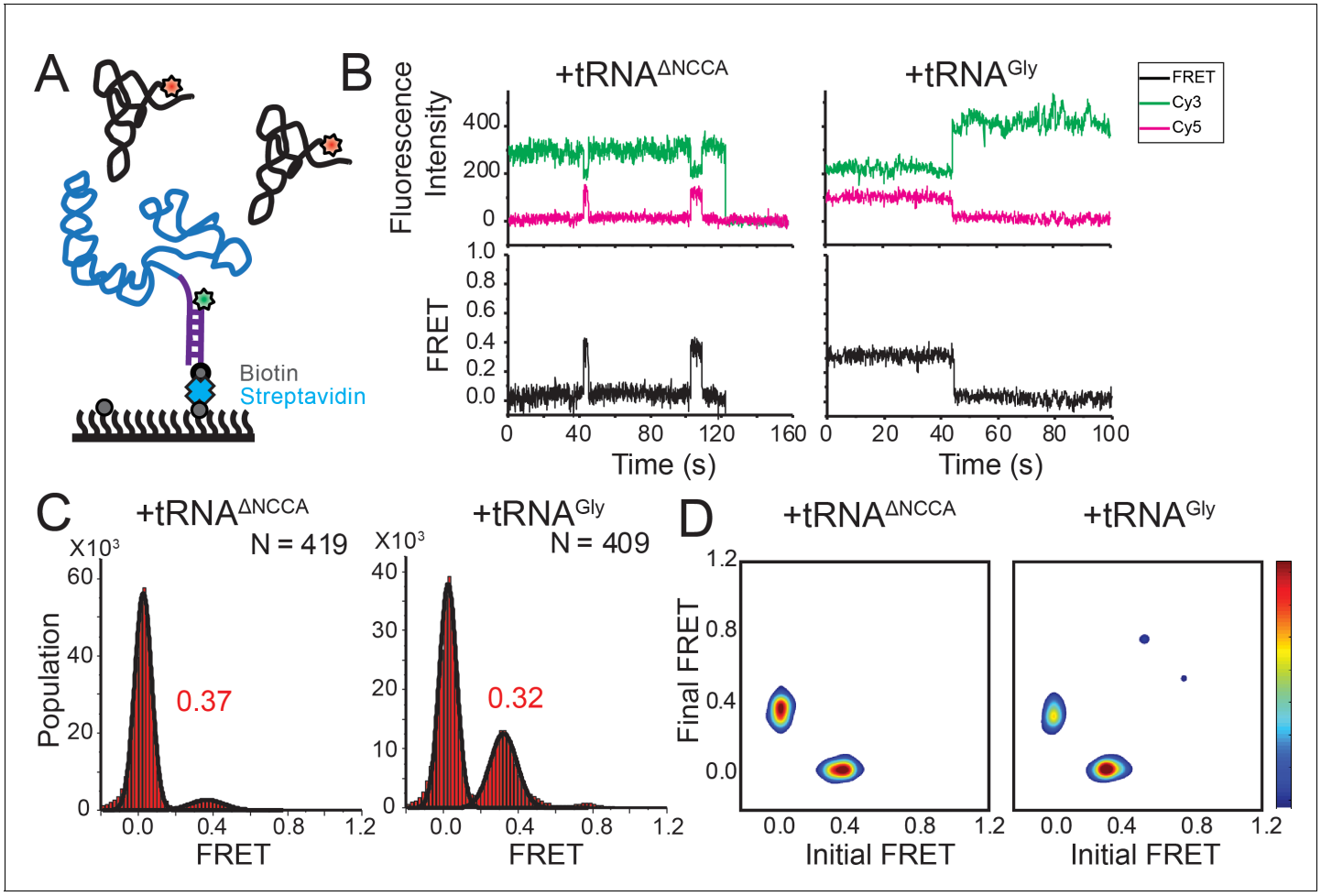

Figure 4. FRET between fluorophores at the 5′ end of the *glyQS* T-box riboswitch and 5′ end of $tRNA^{Gly}$ is insensitive to the two binding states. (**A**) Cy3 (green star) and Cy5 (red star) are attached at the 5′ extension of the T-box (blue) and the 5′ of the tRNA (black), respectively. (**B**) smFRET trajectories of T-box-Cy3(5′) with $tRNA^{\Delta NCCA}$-Cy5 (left) and $tRNA^{Gly}$-Cy5 (right). 'N' denotes the total number of traces in each histogram from three independent experiments. (**C**) One-dimensional FRET histograms of T-box-Cy3(5′) with $tRNA^{\Delta NCCA}$-Cy5 (left) and $tRNA^{Gly}$-Cy5 (right). (**D**) TDP of T-box-Cy3(5′) with $tRNA^{\Delta NCCA}$-Cy5 (left) and $tRNA^{Gly}$-Cy5 (right). Contours are plotted in the same way as in ***Figure 2D***. TDPs are generated from all smFRET traces from three independent experiments.

DOI: https://doi.org/10.7554/eLife.39518.024

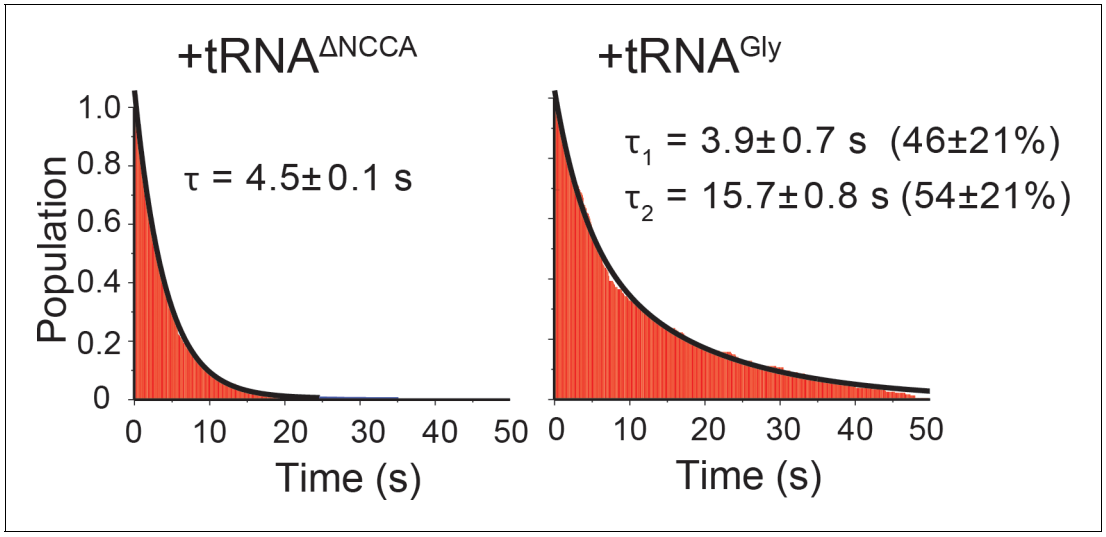

Figure 4—figure supplement 1. Lifetime analyses of *glyQS* T-box-Cy3(5') and tRNA-Cy5 interaction. Dwell time of bound state in the presence of $tRNA^{\Delta NCCA}$-Cy5 (left) is fit with a single-exponential decay function (black curve). Dwell time of the bound state in the presence of $tRNA^{Gly}$-Cy5 (right) is fit with double exponential decay function (black curve). Mean ±S.D. are calculated from three independent measurements.

DOI: https://doi.org/10.7554/eLife.39518.025

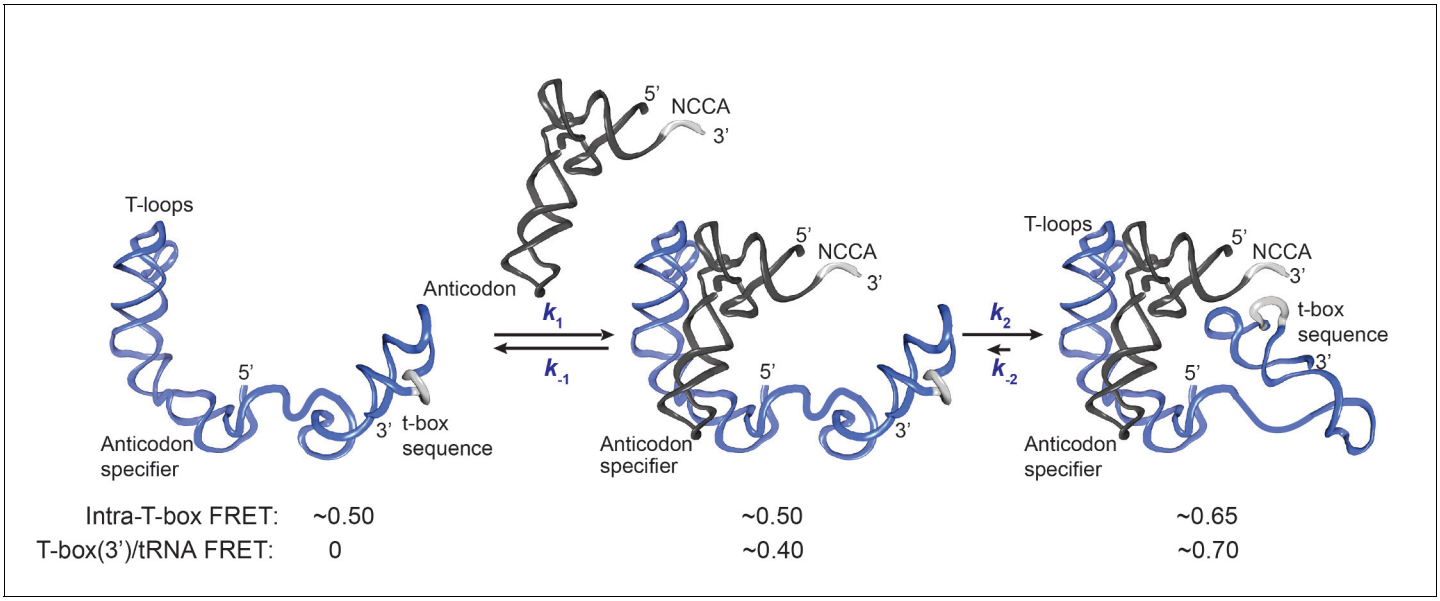

Figure 5. Kinetic model for the two-step binding of *glyQS* T-box riboswitch and uncharged $tRNA^{Gly}$. Details of the model are described in the text. Rate constants are summarized in ***Figure 6E***.

DOI: https://doi.org/10.7554/eLife.39518.028

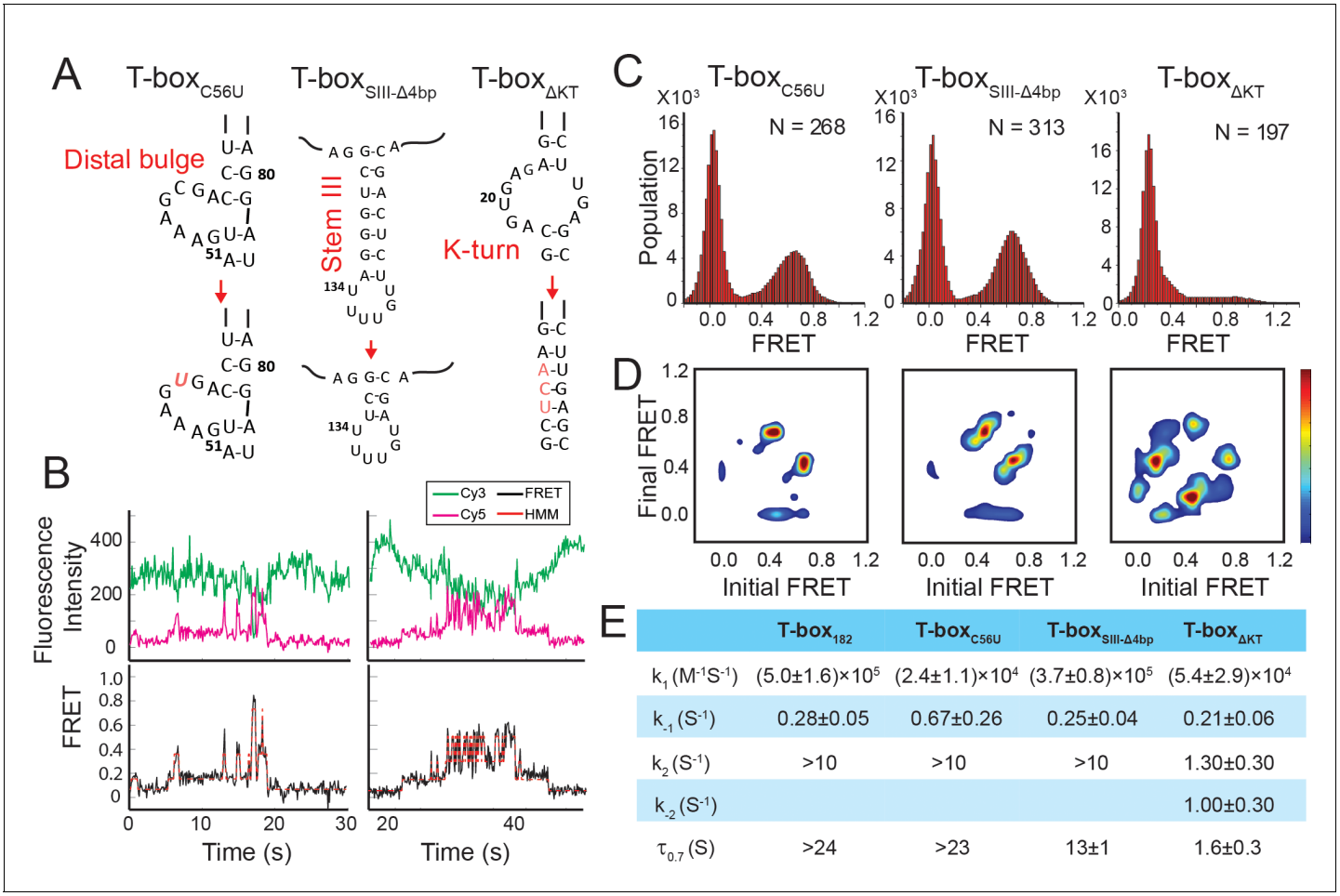

	T-box$_{182}$	T-box$_{C56U}$	T-box$_{SIII-\Delta4bp}$	T-box$_{\Delta KT}$
k_1 ($M^{-1}S^{-1}$)	$(5.0\pm1.6)\times10^5$	$(2.4\pm1.1)\times10^4$	$(3.7\pm0.8)\times10^5$	$(5.4\pm2.9)\times10^4$
k_{-1} (S^{-1})	0.28±0.05	0.67±0.26	0.25±0.04	0.21±0.06
k_2 (S^{-1})	>10	>10	>10	1.30±0.30
k_{-2} (S^{-1})				1.00±0.30
$\tau_{0.7}$ (S)	>24	>23	13±1	1.6±0.3

Figure 6. Regulation of the tRNA^{Gly} binding kinetics by structural elements in the *glyQS* T-box riboswitch. (**A**) Schematic diagram of three different mutations introduced to the T-box$_{182}$ backbone (T-box$_{C56U}$, T-box$_{SIII-\Delta4bp}$ and T-box$_{\Delta KT}$). (**B**) Representative smFRET traces of T-box$_{\Delta KT}$-Cy3(3′) and tRNA^{Gly}-Cy5. (**C**) FRET histograms of the T-box mutants with tRNA^{Gly}-Cy5. 'N' denotes the total number of traces in each histogram from three independent experiments. (**D**) TDP of the T-box mutants with tRNA^{Gly}-Cy5. TDPs are generated from all smFRET traces from three independent experiments and are plotted in the same way as in ***Figure 2D***. (**E**) Table of kinetic parameters for tRNA^{Gly}-Cy5 binding to different T-box constructs. k_{-1}, k_2, and k_{-2} of T-box$_{\Delta KT}$-Cy3(3′) are apparent rate constants estimated to allow comparison as described in Materials and methods. All rate constants are reported as mean ± standard deviation (S.D.) from three or four independent experiments.

DOI: https://doi.org/10.7554/eLife.39518.029

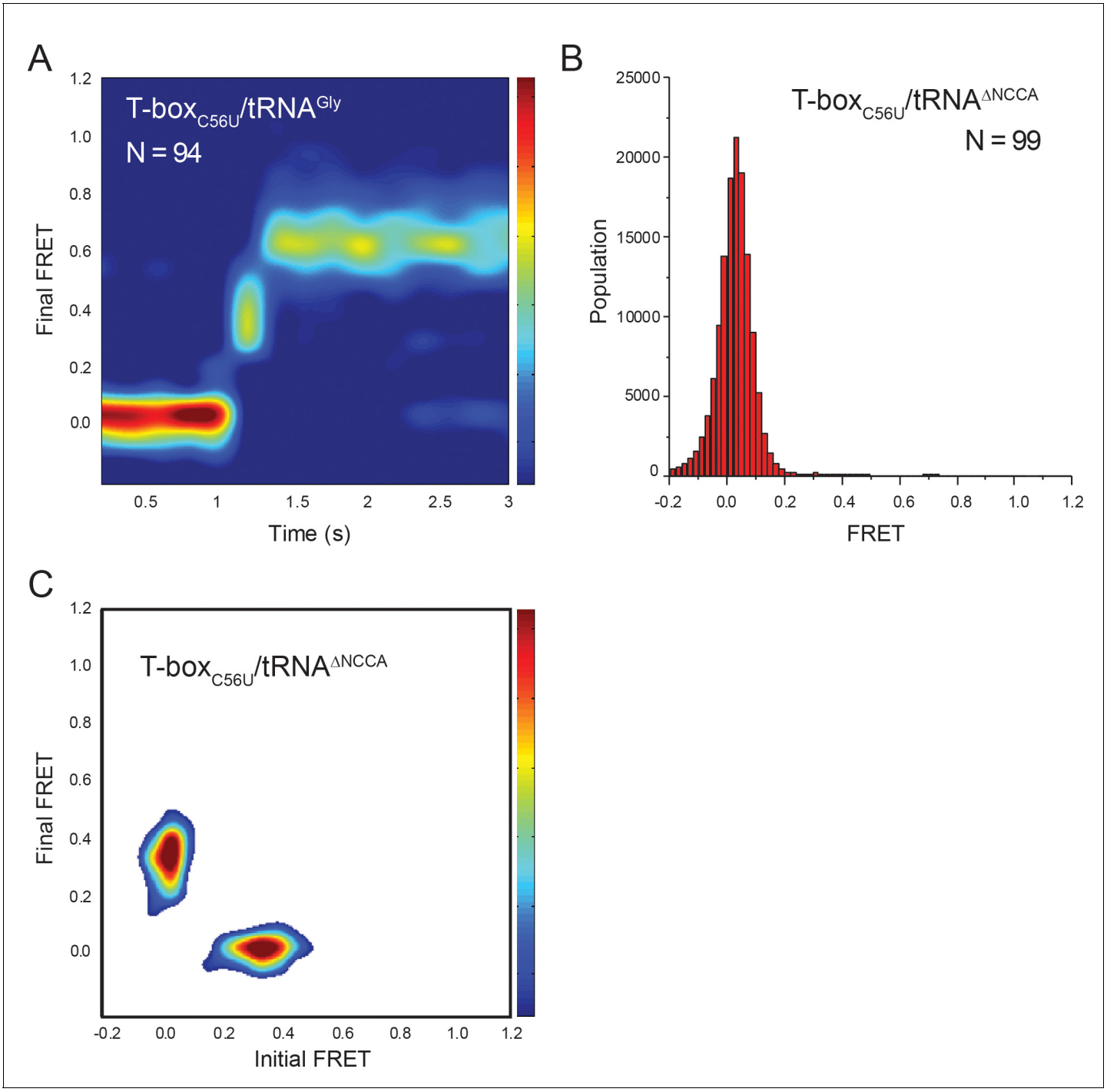

Figure 6—figure supplement 1. tRNA-Cy5 binding to T-box$_{C56U}$-Cy3(3′). (**A**) Surface contour plot of time-evolved FRET histogram of T-box$_{C56U}$-Cy3(3′) with tRNA^{Gly}-Cy5 with traces showing real-time binding. Contours are plotted in the same way as in ***Figure 2F***. 'N' denotes the total number of traces in each histogram from three independent experiments, which are a subset of traces showing real-time binding event in the steady-state measurements. Total number of traces in the steady-state measurements is indicated in ***Figure 6C***. (**B**) FRET histogram of T-box$_{C56U}$-Cy3(3′) with tRNA$^{\Delta NCCA}$-Cy5. 'N' denotes the total number of traces three independent experiments. (**C**) TDP of T-box$_{C56U}$-Cy3(3′) with tRNA$^{\Delta NCCA}$-Cy5. TDP is generated from all smFRET traces from three independent experiments and is plotted in the same way as in ***Figure 2D***.

DOI: https://doi.org/10.7554/eLife.39518.030

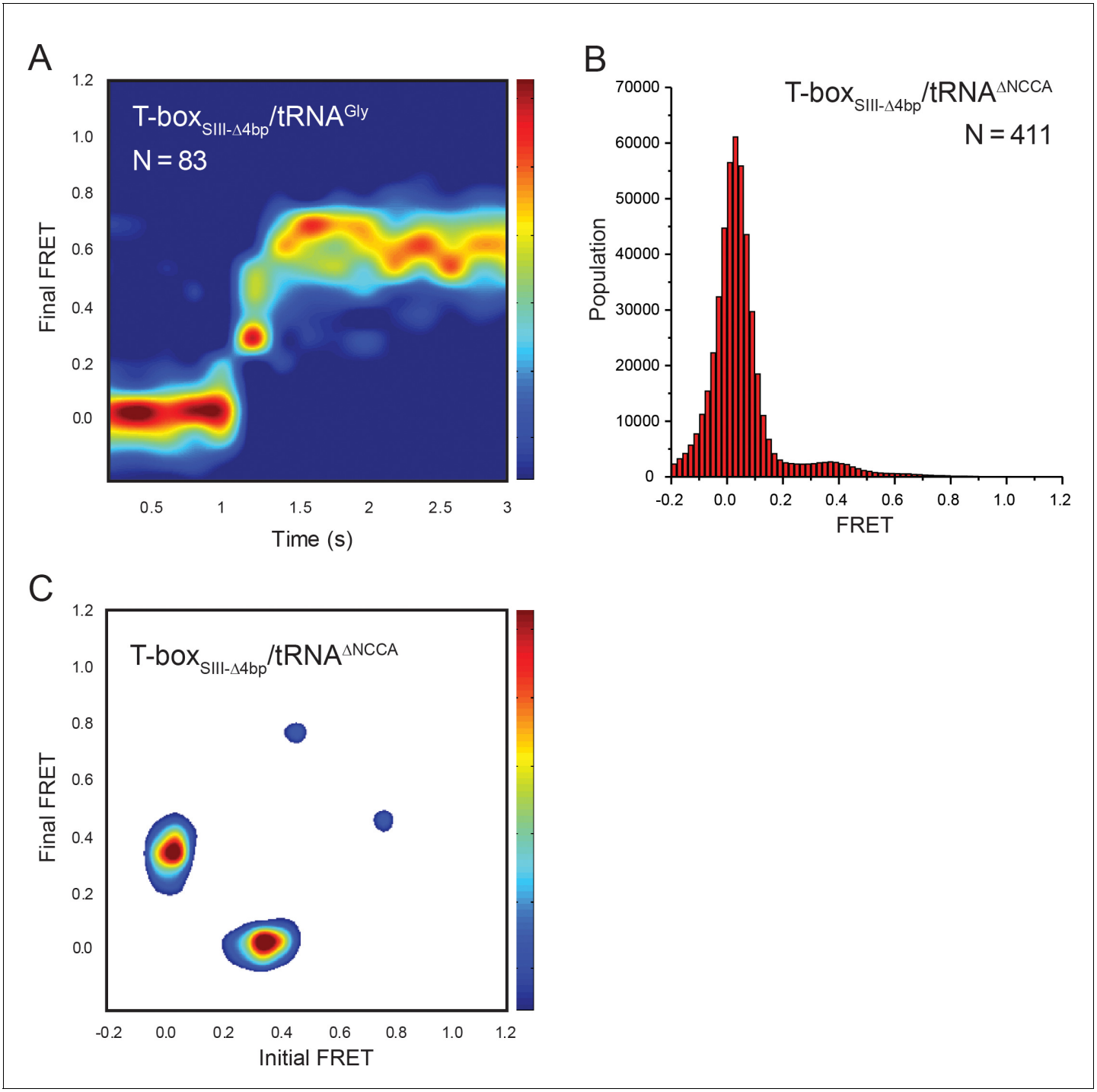

Figure 6—figure supplement 2. tRNA-Cy5 binding to T-box$_{SIII-\Delta4bp}$-Cy3(3′). (**A**) Surface contour plot of time-evolved FRET histogram of T-box$_{SIII-\Delta4bp}$-Cy3(3′) with tRNA^{Gly}-Cy5 with traces showing real-time binding. Contours are plotted in the same way as in ***Figure 2F***. 'N' denotes the total number of traces in each histogram from three independent experiments, which are a subset of traces showing real-time binding event in the steady-state measurements. Total number of traces in the steady-state measurements is indicated in ***Figure 6C***. (**B**) FRET histogram of T-box$_{SIII-\Delta4bp}$-Cy3(3′) with tRNA$^{\Delta NCCA}$-Cy5. 'N' denotes the total number of traces from four independent experiments. (**C**) TDP of T-box$_{SIII-\Delta4bp}$-Cy3(3′) with tRNA$^{\Delta NCCA}$-Cy5. TDP is generated from all smFRET traces from four independent experiments and is plotted in the same way as in ***Figure 2D***.

DOI: https://doi.org/10.7554/eLife.39518.031

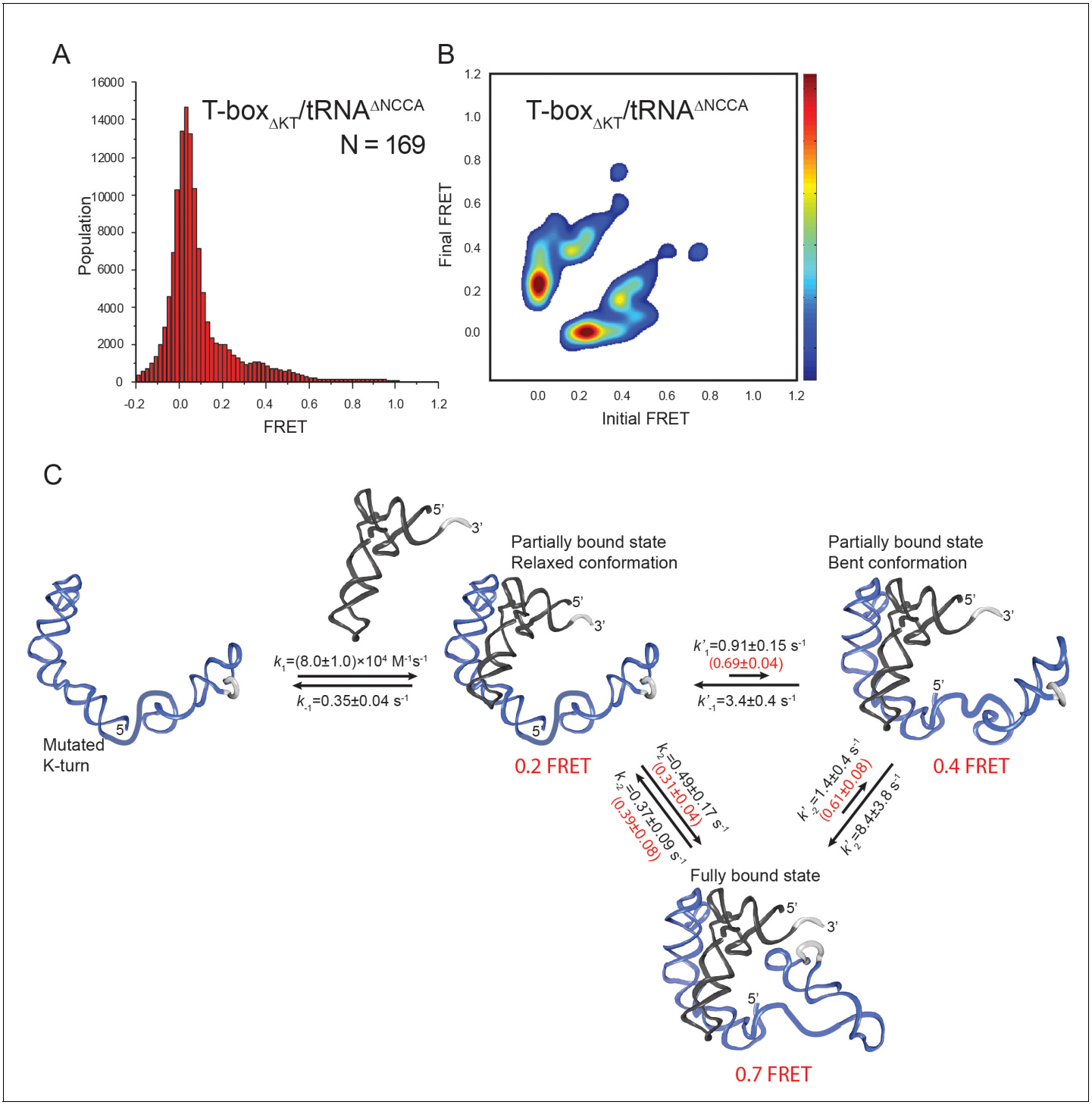

Figure 6—figure supplement 3. tRNA-Cy5 binding to T-box$_{\Delta KT}$-Cy3(3′). (**A**) FRET histogram of T-box$_{\Delta KT}$-Cy3(3′) with tRNA$^{\Delta NCCA}$-Cy5. 'N' denotes the total number of traces from three independent experiments. (**B**) TDP of T-box$_{\Delta KT}$-Cy3(3′) with tRNA$^{\Delta NCCA}$-Cy5. TDP is generated from all smFRET traces from three independent experiments and is plotted in the same way as in ***Figure 2D***. (**C**) Kinetic model of tRNA^{Gly} binding to T-box$_{\Delta KT}$. Transition rate constants are reported as mean ±S.D from three independent measurements. Probabilities of different pathways for transitioning into and out of 0.7 FRET states are marked in red in parenthesis.

DOI: https://doi.org/10.7554/eLife.39518.032

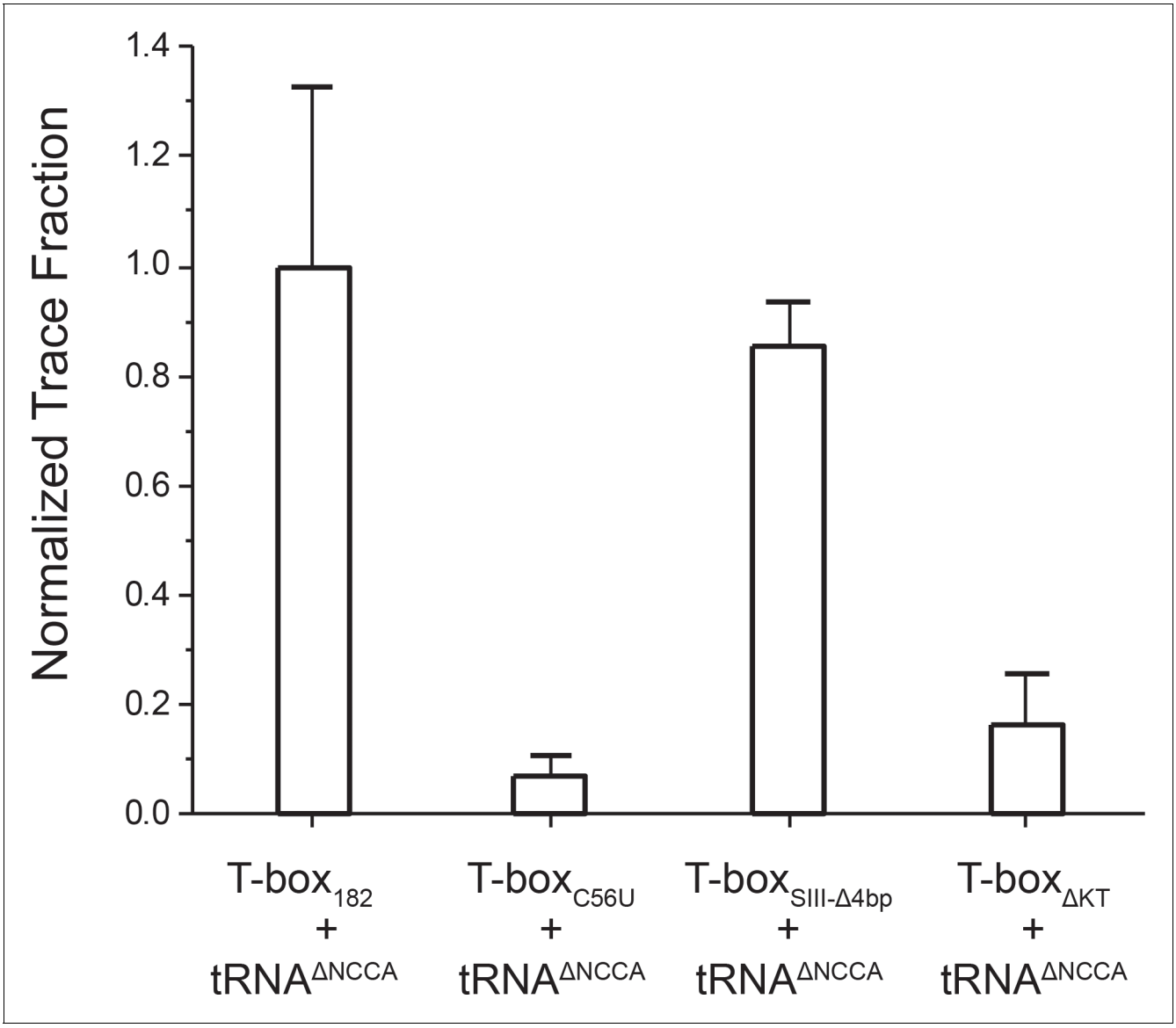

Figure 6—figure supplement 4. Normalized FRET trace percentage of T-box-Cy3(3′) and $tRNA^{\Delta NCCA}$-Cy5. The error bars correspond to the standard deviations from 3 or four independent measurements.

DOI: https://doi.org/10.7554/eLife.39518.033

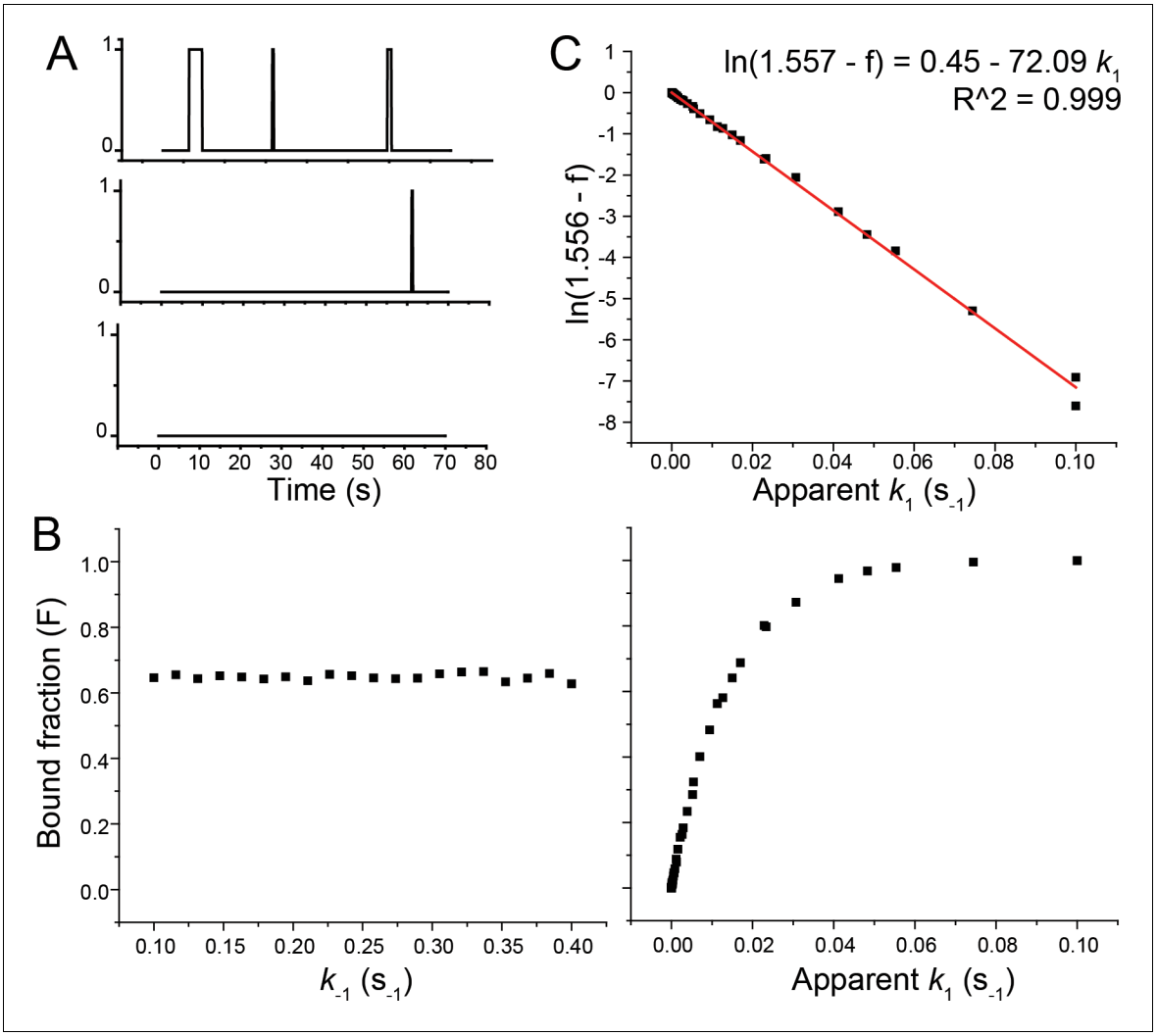

Figure 6—figure supplement 5. Determination of k_1. (**A**) Examples of binding traces simulated by the Gillespie algorithm (***Gillespie, 1976***; ***Gillespie, 1977***; ***Gillespie, 2007***). '1' represents a binding event, and '0' represents the unbound state. If there is a single binding event within the 70 s time window, the trace is included in the bound fraction (*F*). *F* is defined by the number of traces showing a binding event divided by the total number simulated traces. (**B**) Simulation of *F* as a function of k_{-1}, where apparent k_1 is set to be 0.015 s^{-1}, to be consistent with our measured apparent k_1 in the presence of 30 nM tRNA on WT T-box$_{182}$ (left panel). Simulation of *F* as a function of apparent k_1, where k_{-1} is set to be 0.25 s^{-1} to be consistent with our measured k_{-1}. (**C**) Normalized bound fraction (*f*) is *F* normalized to the value at apparent k_1 = 0.015 s^{-1}, to reflect the equivalent quantification of normalized trace fraction to the case of tRNA binding to WT T-box$_{182}$ (***Figure 6—figure supplement 4***). Red line presents the linear fitting of ln(f_0-*f*) *vs.* apparent k_1.

DOI: https://doi.org/10.7554/eLife.39518.034